Malaysian Journal of Chemistry, 2022, Vol. 24(4), 215-230
*(*Special Issue: *2nd International Conference on Innovative Sciences & Technology for Research & Education 2022)*

Superabsorbent Interpenetrating Polymer Networks for Adsorption of Organic Dyes from Aqueous Solutions

Hikmat Hidayat Muhammad Rapaiee[1], Cindy Soo Yun Tan[1]*, Dzureen Julaihi[1], Heather Lambi Apong[1], Siong Fong Sim[2], Fui Kiew Liew[1], Yanti Yana Halid[1], Chel-Ken Chiam[3] and Leslie Thian Lung Than[4]

[1]Faculty of Applied Sciences, University Teknologi MARA, 94300 Kota Samarahan, Sarawak, Malaysia
[2]Faculty of Resource Science and Technology, Universiti Malaysia Sarawak, 94300 Kota Samarahan, Sarawak, Malaysia
[3]Faculty of Engineering, Universiti Malaysia Sabah, Jalan UMS, 88400 Kota Kinabalu, Sabah
[4]Department of Medical Microbiology, Faculty of Medicine and Health Sciences, Universiti Putra Malaysia, 43400 UPM Serdang, Selangor
*Corresponding author (e-mail: cindytan@uitm.edu.my)

Superabsorbent interpenetrating polymer networks (IPN) consisting of PVA/PAA-HA (two-component) and PVA/PAA-HA/P(AAm-*co*-VIm) (three-component) were synthesized through free-radical polymerization and assembled via polymer blending in aqueous solutions followed by cyclic freeze-thaw. The polymers and polymer network assemblies were systematically characterized by FTIR, NMR and FESEM and were investigated for organic dyes adsorption. The IPN hydrogels were strong and stable adsorbents based on their mechanical rigidity and dimension. Excellent swelling percentages (>3000 %) in DI water indicated their superabsorbent properties owing to the hydrophilic polymers, leading to the pore opening within the swollen IPN adsorbents, which facilitates the cationic methylene blue (MB) adsorption onto the adsorbents. In contrast to the low removal of anionic methyl orange (MO) dye, high removal percentages (>90%) and adsorption capacities (~230 mg g^{-1}) observed for MB dye by both PVA/PAA-HA and PVA/PAA-HA/P(AAm-*co*-VIm) adsorbents suggested selective chemisorption towards cationic species, which corresponded to the pseudo-second order kinetic model. The fitting of the experimental adsorption data indicates different adsorption isotherms of MB for the IPN adsorbents. Whilst the PVA/PAA-HA adsorbent obeyed the Langmuir model, the PVA/PAA-HA/P(AAm-*co*-VIm) adsorbent followed the Freundlich model for the MB adsorption in aqueous solutions.

Key words: Interpenetrating polymer networks; adsorbents; adsorption; organic dyes; methylene blue; methyl orange

Received: September 2022; Accepted: November 2022

High volume of wastewaters is generated from a variety of domestic and industrial activities daily. These industrial discharges often contain a wide array of recalcitrant and hazardous heavy metals, dyes, and pathogens which tend to accumulate in the biosphere and aquatic organisms and unwittingly make their way back through human diet, thus pose health consequences [1]. With continuous industrial development, organic dyes and other colouring agents are widely used in textile, food processing, leather, paper making and printing industries, resulting in increasing discharges of coloured effluents [2]. Untreated dye discharges and wastewaters can attribute to serious water pollution due to their non-biodegradable, carcinogenic and highly toxic natures [3]. Organic dyes, such as azo and thiazine dyes, are extremely hazardous waste toxins for both humans and animals, even in low concentrations. Azo dyes (e.g. methyl orange, tartrazine) contain a non-degradable azo linkage (R-N=N-R'), where R and R' are usually aryl groups, whereas thiazine dyes, such as methylene blue, are a class of electron-rich tricyclic nitrogen–sulphur heterocycles [4]. From the toxicological and ecological perspectives, it is therefore essential to treat effluents containing these dyes.

Adsorption is a widely favoured technique to remove water-soluble pollutants on account of its simplicity, cost-efficiency, adsorbent recyclability and the availability of a wide range of adsorbents [5-6]. Despite extensive development of adsorbents for water remediation, existing adsorbents suffer from lack of pollutant selectivity, low separation efficiency, generation of secondary pollution and are unable to handle large sample volume, leading to challenges and impracticality of these sorbents in real-life applications [3]. An array of functional adsorbents and smart adsorbents, including activated carbon, clay, carbon nanotubes, biomass, ion-exchange resins, polymer composites and hydrogels have been reported for emerging aquatic pollutants removal [5-8].

†Paper presented at the 2nd International Conference on Innovative Sciences & Technology for Research & Education 2022

Polymeric materials in various physical forms, such as membranes, hydrogels, nanocomposites and electrospun nanofibers, play a vital role in wastewater treatment applications [9]. Functional hydrogels and polymer networks have gained great attention as effective adsorbents because their physico-chemical and bulk mechanical properties can be designed and tailored to enhance their mechanical durability and adsorption capacities at lower costs. A variety of chemical functionalities containing oxygen (O), nitrogen (N) and/or thiol (S) groups into the polymeric adsorbents are incorporated into the polymer-based adsorbents via facile synthesis. However, uncrosslinked traditional hydrogels and superabsorbent materials, such as acrylate-based polymers, have demonstrated low mechanical integrity and uncontrolled swelling behaviour, thus are prone to dissolution or breakage, making them unsuitable to be used as adsorbent candidates. On account of unavailable adsorptive/ functional sites within these poor three-dimensional polymer structures, low adsorption capacities have been reported [3]. To-date, it remains a great challenge to scientists to achieve a mechanically robust polymeric adsorbent which fulfils the requirements of high adsorption capacity, fast kinetics, excellent selectivity towards specific contaminants and recyclability by using an individual material [10].

Hydrogels with high modulus and super-absorbent properties can be obtained by inter-penetrating a tightly crosslinked first polymer network with a loosely crosslinked second polymer network without any covalent bonds between them. The denser interpenetrating polymer network (IPN) hydrogels possess more distinct benefits as multifunctional adsorbents compared to single-network hydrogels. The IPN hydrogels are endowed with excellent adsorption kinetics for ionic species like heavy metals and dyes [11]. Hu et al. [12] reported enhanced and rapid methylene blue adsorption triggered by the phase transition of the thermoresponsive and porous hybrid IPN alginate–Ca^{2+}/ P(MEO_2MA-*co*-$OEGMA_{300}$)/*g*-C_3N_4 hydrogel compared to other hydrogels and pure *g*-C_3N_4 nanosheets. Another study reported a novel poly(acrylic acid)-based super-adsorbent nanocomposite hydrogels containing non-aggregated calcium hydroxide ($Ca(OH)_2$) nano-spherulites with maximum adsorption capacity for methylene blue higher than 2000 mg g^{-1} [3]. Sarmah & Karak (2020) synthesized an amphoteric double network hydrogel consisting of covalently crosslinked starch and poly(acrylic acid) which could adsorb both cationic dye (methylene blue) and anionic dye (congo red) with adsorption maxima of 133.65 mg/g and 64.73 mg/g, respectively [13]. A novel triptycene-based hyper-crosslinked porous polymer (TPP–PP), which was synthesized by a Friedel–Crafts reaction, exhibited high adsorption capacities for methyl orange (220.82 mg g^{-1}) and methyl blue (159.80 mg g^{-1}) solutions (He at al., 2022) [14]. Magnetic hydrogel beads based on poly(vinyl alcohol)/carboxymethyl starch-*g*-poly(vinyl imidazole) were also reported for the removal of dyes and heavy metal ions [15].

This study focuses on the synthesis of super-absorbent IPN hydrogels containing loosely cross-linked sodium humate grafted poly(acrylic acid) (PAA-HA), poly(acrylamide-*co*-1-vinylimidazole) (P(AAm-*co*-VIm)) and commercially available poly (vinyl alcohol) (PVA). Both PAA-HA and P(AAm-*co*-VIm) were synthesized via random free-radical polymerization separately (Figure 1a). These polymers were then blended with PVA in aqueous solution and subjected to cyclic freeze-thawing to assemble as two-component and three-component IPN adsorbents for removal of organic dyes (Figure 1b). Swelling behaviour in different media at pH 7 and surface morphology of the PVA/PAA-HA and the PVA/PAA-HA/P(AAm-*co*-VIm) IPN adsorbents were investigated. Effects of adsorbent dosage, initial dye concentrations and time-dependent adsorption of a cationic (methylene blue, MB) and anionic (methyl orange, MO) organic dyes were studied and compared in batch experiments. Possible mechanisms through which the MB dye adsorbed onto the IPN adsorbents were also discussed in light of the adsorption kinetics and isotherms of the dye.

EXPERIMENTAL

Materials

Polyvinyl alcohol (PVA) (99% hydrolyzed average MW of 130 000 g mol^{-1}), acrylic acid (AA, anhydrous, 99%), sodium humate (HA, technical grade), *N*,*N*-methylenebis(acrylamide) (MBA, 99%), 4,4′-azobis (4-cyanopentanoic acid) (ACPA, 98%), acrylamide (AAm, 98%), methylene blue hydrate (MB, anhydrous, >95%) and, methyl orange (MO, 85%) were purchased from Sigma Aldrich (Germany) and used without further purification. Ammonium persulfate (APS, 98%) was purchased from Acros Organics. 1-vinylimidazole (VIm) was purchased from China.

Synthesis of Sodium Humate Grafted Poly(acrylic acid), PAA-HA

PAA-HA with a degree of neutralization (60%) was synthesized in the reaction mixture containing AA monomer (10 g). NaOH (8 M) and DI water (7 mL) were added to a 50-mL two-neck round bottom flask. HA (0.3 g) was dissolved in DI water (10 mL). Then, MBA (0.015 g) and HA were added under stirring of 300 rpm. APS (0.07 g) was added as the free-radical polymerization initiator, and the reaction mixture was left under constant stirring in N_2 atmosphere for 30 min before transferring it in an oil bath at 70 °C for 1 h. A black translucent polymer was yielded, which was washed with copious amount of DI water to remove the unreacted reactants and oven dried at 60 – 70 °C. The yield of dried black polymer was 14.35 g and 100 % conversion of monomer to polymer was observed. The dried PAA-HA was used for characterization and formation of two- as well as three-component polymer networks.

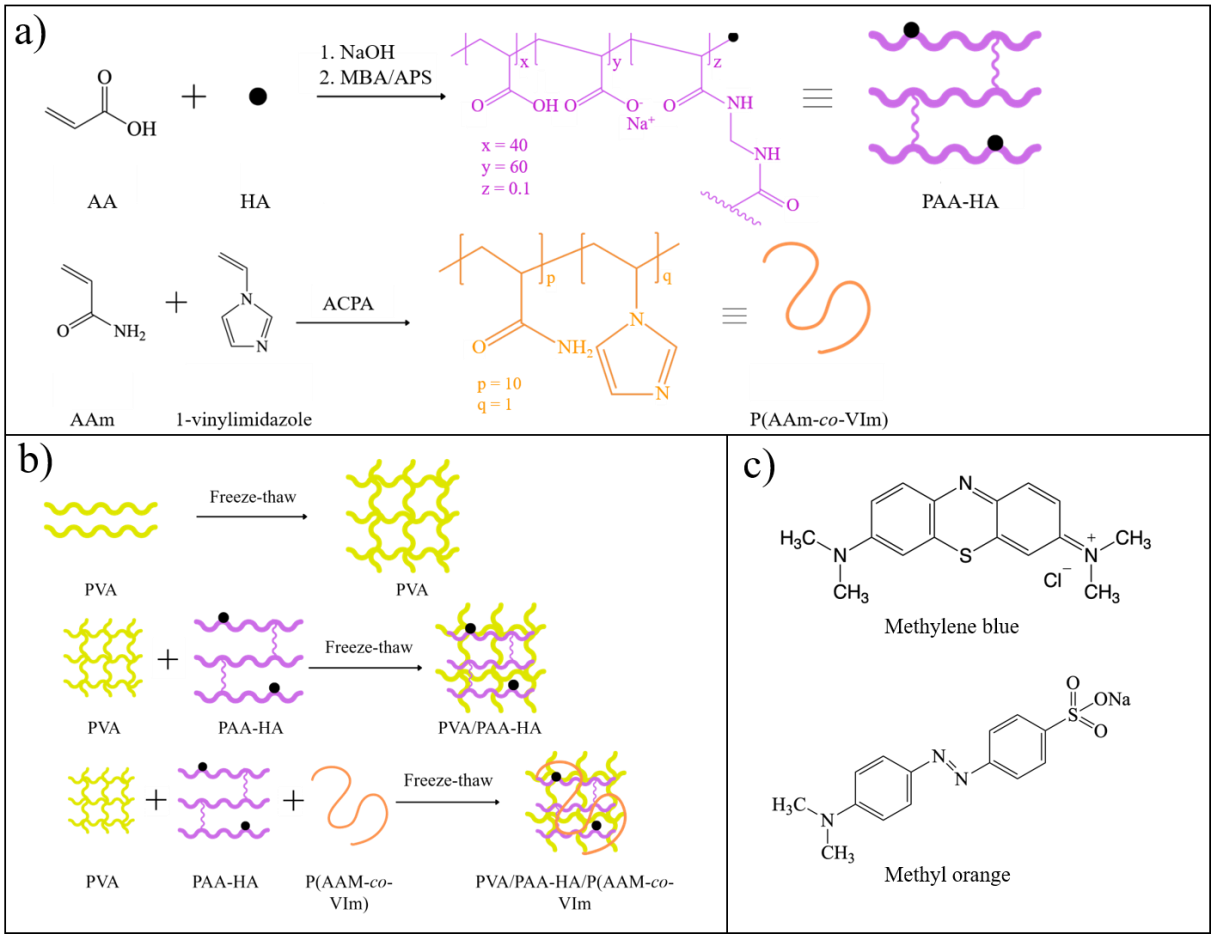

Figure 1. (a) Synthesis of PAA-HA and P(AAm-*co*-VIm) polymers; (b) schematic representation of single-, two- and three-component interpenetrating polymer networks (IPN) formation; and (c) chemical structures of methylene blue and methyl orange dyes.

Synthesis of Poly(acrylamide-*co*-1-vinylimidazole), P(AAm-*co*-VIm)

AAm monomer (10 g) and VIm (3.3 g) were added to a 50-mL two-neck round bottom flask and DI water (75 mL) was added to the flask. The reaction mixture was stirred under N_2 for 30 min at room temperature. Next, ACPA (0.49 g) was added to the solution as the initiator for the random free-radical polymerization, and was stirred under N_2, before transferring it to the oil bath at 60 °C for 24 h under constant stirring. The resultant polymer was precipitated in acetone to obtain an amorphous white powder, dried to a constant weight at 45 °C and milled. 16.54 g of dried P(AAm-*co*-VIm) was yielded. The dried P(AAm-*co*-VIm) was used for characterization and formation of three-component polymer network.

Preparation of Single-component Polymer Network, PVA

PVA (2 g) was dissolved in DI water (40 mL), stirred at 90 °C until a homogenous solution containing 5% PVA was obtained. The PVA solution was poured into a 1 cm^3 silicon mould, frozen at -20 °C for 18 h and thawed at room temperature for 4 h for three consecutive freeze-thaw cycles. After that, the PVA hydrogels were oven dried at 45 °C until constant weight. Average weight of a dried PVA cube was 62.80 ± 1.45 mg.

Preparation of Two-component Interpenetrating Polymer Network, PVA/PAA-HA

PVA solution (5%) was prepared in DI water following the previous method. PAA-HA (0.8 g) was added to the solution under continuous heating and stirring until it was completely dissolved. The weight ratio of PVA:PAA-HA was 5:2. The PVA/PAA-HA solution was poured into the 1 cm^3 silicone mould, frozen at -20 °C for 18 h and thawed at room temperature for 4 h for three freeze-thaw cycles. The PVA/PAA-HA mixture was then oven dried at 45 °C until constant weight. Average weight of a dried PVA/PAA-HA IPN cube was 87.23 ± 1.33 mg.

Preparation of Three-component Interpenetrating Polymer Network, PVA/PAA-HA/P(AAm-*co*-VIm)

Three-component polymer networks were prepared, with the dissolution of PVA (5%) and P(AAm-*co*-VIm) (3%) in DI water separately at 90 °C. P(AAm-*co*-VIm) solution was then added to the PVA solution, followed by the PAA-HA solution (2% w/v) while stirring until a uniform PVA/PAA-HA/P(AAm-*co*-VIm) dispersion was obtained. The mixture was poured into the 1 cm^3 silicone mould, frozen at -20 °C for 18 h and thawed at room temperature for 4 h for three freeze-thaw cycles and oven dried at 45 °C until constant weight. Average weight of a dried PVA/PAA-HAA/ P(AAm-*co*-VIm) IPN cube was 113.60 ± 1.95 mg.

Characterization

The synthesized polymers and polymer networks were characterized by using ATR-FTIR Spectrometer (Perkin Elmer, Frontier model) within 4000 – 600 cm^{-1}. The FTIR analysis was carried out to study the chemical functionalities of polymers. The polymers were dissolved with suitable deuterated solvents and analyzed by using NMR spectrometer (Bruker 400 MHz) to confirm their chemical structures. Surface morphology of polymer networks were observed under a Field Emission Scanning Electron Microscope (FESEM, model JSM-IT500HR, JEOL, Japan) after being sputtered with gold.

Swelling Behaviour Analysis

Swelling behaviour of PVA/PAA-HA and the PVA/PAA-HA/P(AAm-*co*-VIm) polymer networks were investigated based on weight differences of the dried and swollen adsorbents. The dried PVA/PAA-HA cubes were immersed in DI water and phosphate buffer solution (PBS, 50 mL) separately at room temperature and pH 7 until they reached equilibrium. After that, the swollen hydrogels were weighed after removing excess water from the surface of the adsorbents with Whatman filter paper. The weight of adsorbents were recorded hourly for the first 6 h, followed by 24 h, 48 h and 168 h. The equilibrium swelling ratio of the adsorbents was calculated using Equation 1. This swelling experiment was repeated for the PVA/PAA-HA/P(AAm-*co*-VIm) adsorbents under similar conditions. The swelling experiment were conducted in triplicates.

$$\text{Equilibrium swelling (\%)} = \frac{(W_s - W_d)}{W_d} \times 100 \qquad \text{Equation 1}$$

where, W_d = the weight of dried adsorbent and W_s = the weight of swollen adsorbent.

Adsorption Experiments

Dye adsorption of the polymer adsorbents were carried out in batch experiments, and were immersed in a series of model organic dyes. Methylene blue (MB) was used as the model cationic organic dye, while methyl orange (MO) was the model anionic organic dye (Figure 1c). The adsorbent dosage refers to the amount of adsorbent (in unit g) used per volume of solution (in unit L). Different adsorbent dosages (Table 1) were used in the batch adsorption experiments to determine the most suitable amount of adsorbent for adsorption kinetics and isotherm studies.

Table 1. Experimental parameters for dye batch adsorption studies. The batch adsorption experiments were carried out until adsorption equilibrium was achieved for each adsorbent.

Adsorbent dosage (g L^{-1})	Volume of dye solution (mL)	Weight of adsorbent (mg)	Initial dye concentration (mg L^{-1})	Dye
1.0	100	100	250	**MB, MO**
2.0	100	200	250	
1.0	100	100	50 100 150 200 250 300 **350** **400** **450** **500**	**MB**

Predetermined amounts of dried PVA/PAA-HA and PVA/PAA-HA/P(AAm-*co*-VIm) adsorbents were weighed and immersed in MB and MO solutions (250 ppm, 100 mL) in conical flasks at pH 7, separately. The solution pH was initially adjusted using HCl and NaOH (0.1 M). The solutions were then agitated on a mechanical shaker at 298 K and 150 rpm for 24 h. The concentrations of MB and MO dyes in the supernatant were measured by a UV-Vis Spectrophotometer (Perkin Elmer, Lambda 25) at maximum absorbance of 664 nm and 464 nm, respectively. Standard calibration curves were constructed, and their best fit lines and linear regressions were analysed. The Beer–Lambert Law was used to predict the dye concentration from its absorbance. Dilution was carried out to ensure that the dye concentration was within the limits of standard calibration curves. Each experiment was performed in triplicates under similar experimental conditions.

Adsorption Kinetics and Isotherms of Methylene Blue

The adsorption dosage (1 g L^{-1}) was used for MB adsorption kinetics studies based on its removal efficiency. A series of initial MB concentrations (Table 1, 50 - 500 mg L^{-1}) were used. The adsorbents were placed in the MB solution (pH 7, 298K), followed by mechanical shaking out at various time intervals. The MB concentrations in the supernatants were measured by the UV-Vis spectrophotometer at 664 nm absorbance.

Calculation of Removal Percentages and Equilibrium Adsorption Capacities

Dye removal efficiencies (%) and equilibrium adsorption capacities (q_t, in unit mg g^{-1}) of the adsorbents were calculated using Equations 2 and 3.

$$\text{Removal efficiency (\%)} = \frac{c_o - c_e}{c_o} \times 100\% \qquad \text{Equation 2}$$

$$\text{Equilibrium adsorption capacity, } q_t (\text{mg g}^{-1}) = \frac{(c_o - c_e)V}{m} \qquad \text{Equation 3}$$

where,

q_t = adsorption capacity (mg g^{-1})

c_o = initial concentration of the adsorbate in solution (mg L^{-1})

c_e = equilibrium concentration of the adsorbate in solution (mg L^{-1})

V = volume of dye solution (L)

m = mass of adsorbent (g)

RESULTS AND DISCUSSION

Synthesis and Characterization of Polymers and Polymer Networks

Functional and water-soluble polymers were prepared by using free radical polymerization in aqueous solutions, which include the lightly crosslinked sodium humate grafted poly(acrylic acid) (PAA-HA) and poly(acrylamide-*co*-1-vinylimidazole) (P(AAm-*co*-VIm). AA monomer was 60% neutralized and then poly-merized by using APS initiator in the presence of MBA, (0.1 mol%) and HA to yield a brownish-black PAA-HA. The PAA-HA chains were loosely chemically crosslinked by the MBA crosslinker. During the random free-radical polymerization in the aqueous solution, the brownish-black HA particles were randomly grafted onto the crosslinked PAA chains (PAA-HA). A linear imidazole-containing copolymer, P(AAm-*co*-VIm) was successfully obtained via random free radical copoly-merization of AAm and VIm monomers using ACPA initiator. Due to highly hydrophilic nature, lightly cross-linked PAA-HA and linear P(AAm-*co*-VIm) polymer are soluble in hot DI water.

The ^{1}H NMR spectra of PAA-HA and P(AAm -*co*-VIm) were recorded on an NMR Spectrometer (Bruker, 400 MHz) using D_2O as the solvent (Figure 2). Since NMR analysis could not be carried out for crosslinked PAA-HA most likely due to insoluble HA particles, poly(acrylic acid) (PAA) was synthesized instead under similar polymerization conditions to confirm the chemical structure of the obtained PAA. The yielded PAA was 14.35 g and white in colour. In Figure 2a, the protons H_c (t, 1H) and H_d (d, 2H) of the PAA backbone, were found between 1.00 – 2.20 ppm. The protons from the MBA crosslinker were not visible in this NMR spectrum due to its low amount used (~0.1%). In Figure 2b, the broad peaks at 1.00 – 2.00 ppm (32H) correspond to the H_j, H_k and H_m of P(AAm-*co*-VIm) backbone. Meanwhile, H_h (t, 1H) was shifted to 4.03 ppm due to the neighbouring N atom of the imidazole. The protons H_e (d, 1H), H_f (s, 1H) and H_g (d, 1H) around 7.10 ppm belonged to that of the aromatic imidazole ring. The singlet peak (2H) at 7.70 ppm corresponded to the protons of AAm monomers.

FTIR spectra of the polymers and polymer networks are shown in Figures 3 and 4, respectively. Major absorbance bands for PAA and PAA-HA (Figure 3b-c) were similar, representing their main PAA backbones [16]. Broad O-H stretchings were observed at 3357 – 3366 cm^{-1}, followed by the peaks between 1400 – 1417 cm^{-1} (-OH bending vibration) of the hydroxyl groups. The asymmetric -CH_2 stretching vibration at 2936 cm^{-1} was attributed to the methylene groups of PAA back-bone. The intense -C=O and asymmetrical -COO^- bands of the acrylic acid and acrylate groups in PAA and PAA-HA were observed at 1688 cm^{-1} and 1540 cm^{-1}, respectively. Meanwhile, the bands at 1445 cm^{-1} represented the C-H bending of the polymers. In Figure 3a, prominent absorption peaks arising from HA include -OH stretching (3341 cm^{-1}), -CH_2 stretching (2921 cm^{-1}) and C-O stretching from its phenolic moieties (1100 – 1400 cm^{-1}), which were observed to be hidden by the major peaks of PAA-HA having similar chemical functionalities.

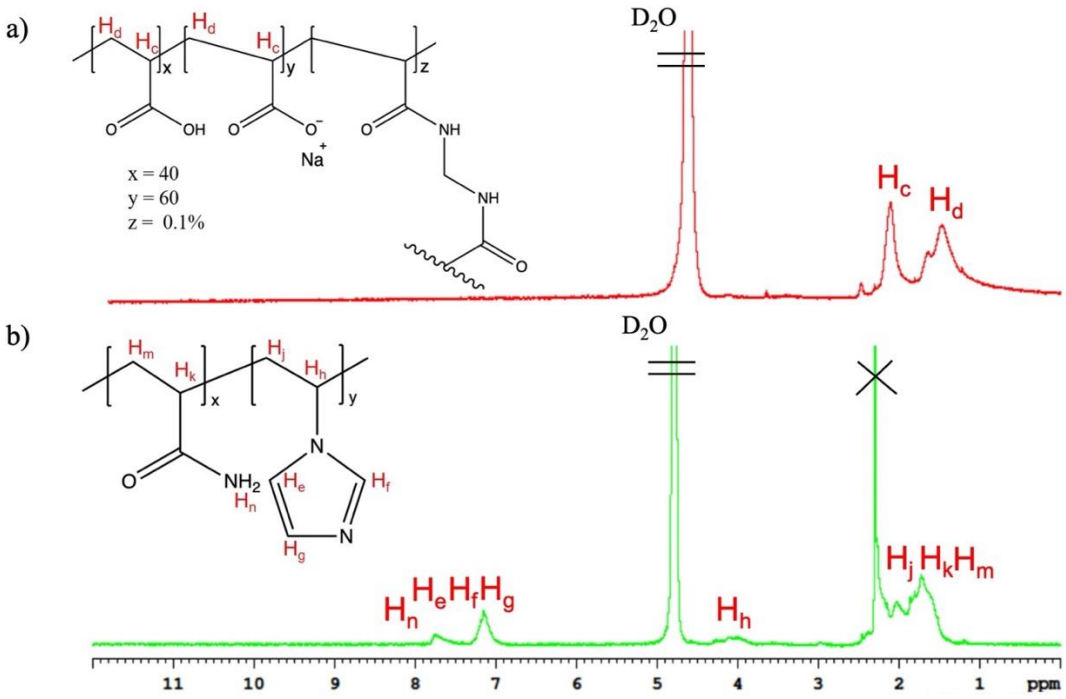

Figure 2. ^{1}H NMR spectra (in D_2O) and chemical structures of (a) PAA which is covalently crosslinked with MBA crosslinker polymer; and (b) P(AAm-*co*-VIm) copolymer.

For P(AAm-*co*-VIm) (Figure 3d), the signals at 3329 cm^{-1} and 3185 cm^{-1} were assigned to the -NH stretching vibration of AAm units which overlapped with the imidazole (VIm) moieties. The smaller peak of C-H stretching was found at 2943 cm^{-1}. The signals between 1600 - 1700 cm^{-1} corresponded to the C=O group of the AAm chain. The absorption bands at 1450 cm^{-1} and 1544 cm^{-1} were ascribed to C–C and N–C stretching vibrations in VIm chain. The absorption bands at 760 and 660 cm^{-1} were assigned to C–H ring bending vibration and C–N vibration of azole ring, respectively. Two other signals at 1285 cm^{-1} and at 1241 cm^{-1}, were attributed to C–H (ring) in-plane bending and C–N (ring) stretching modes, respectively. Based on these characteristic absorption bands of AAm and VIm [15], it was confirmed that P(AAm-*co*-VIm) was synthesized successfully.

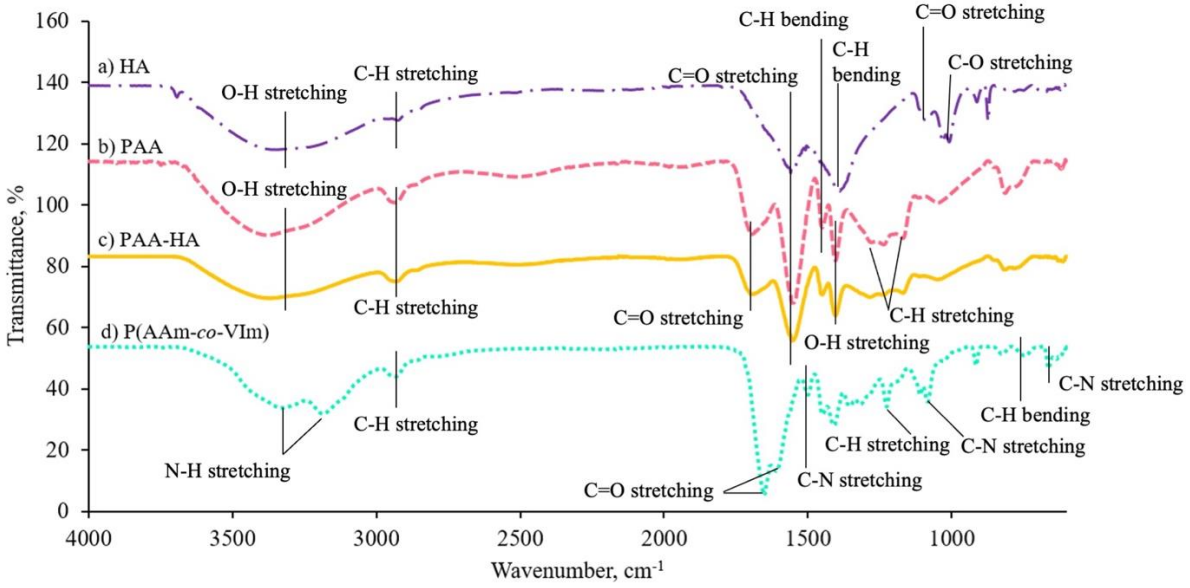

Figure 3. FTIR spectra of (a) sodium humate (HA); (b) PAA; (c) PAA-HA; and (d) P(AAm-*co*-VIm).

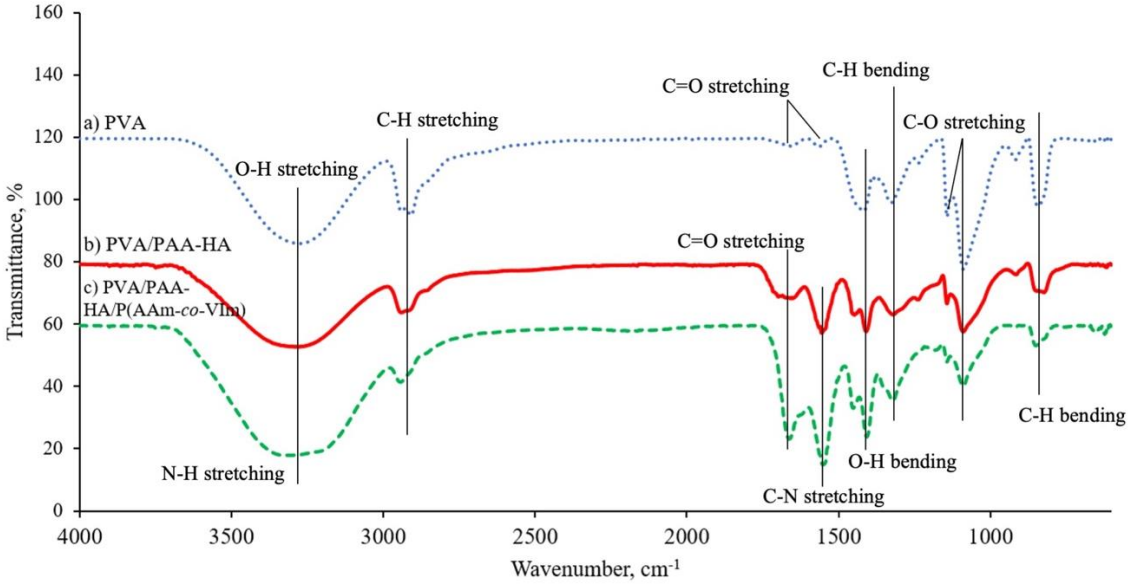

Figure 4. Comparison of FTIR spectra of the polymer networks: (a) single-component PVA; (b) two-component PVA/PAA-HA; and (c) three-component PVA/PAA-HA)/P(AAm-*co*-VIm) polymer networks.

Polymer adsorbents based on IPN concept were assembled from two and three types of functional polymers for adsorption of organic dyes (MB and MO). Herein, a two-component PVA/PAA-HA and three-component PVA/PAA-HA/P(AAm-*co*-VIm) polymer networks were assembled by blending respective polymer solutions according to the weight ratio of 5 : 2 : 3 (PVA/PAA-HA/P(AAm-*co*-VIm). Incorporation of HA particles by grafting onto lightly crosslinked PAA resulted in the dark brown coloured two-component and three-component IPN cubes. In our system, the PAA-HA and PAA-HA/P(AAm-*co*-VIm) acted as the first polymer network, which were intertwined with a second polymer network consisted of PVA, which was then crosslinked via cyclic freeze-thawing. The formed IPN-based adsorbents (Figure 5a, II-III) were observed to have improved structural properties and bulk mechanical strength compared to the single-network PVA adsorbent (Figure 5a, I).

The FTIR spectra of all polymer networks (Figure 4) were analyzed and compared to confirm their successful self-assemblies. In the FTIR spectrum of single-component PVA network (Figure 4a), the signals at 1100 cm^{-1} and 1380 cm^{-1} were attributed to C–O stretching in C–O–H and C–H bending, respectively, while the 1730 cm^{-1} was most likely due to the presence of residual acetate groups in the PVA network. The presence of a band at 1144 cm^{-1} proved that crystallization of the single-component PVA network after cyclic freeze-thaw process involving the C-O stretching band had occurred. This peak is often used to confirmation the PVA structure [15]. Significant O-H and C-H stretching bands were also seen in the PVA network at 3300 cm^{-1} and 2980 cm^{-1}, respectively.

In the FTIR spectrum of two-component PVA/PAA-HA network (Figure 4b), all main absorbance peaks originating from the crystalized PVA and crosslinked PAA/HA polymer could be observed in the two-component PVA/PAA-HA network, indicating that the PVA/PAA-HA interpenetrating polymer network (IPN) was successfully assembled, in which the linear PVA chains were entangled within the covalently crosslinked PAA-HA network when it was added to the PAA-HA solution before it was sent for freeze-thawing to produce the IPN. The broadening peaks at 1709 cm^{-1} and 1659 cm^{-1} were observed to be attributed by C=O stretching of conjugated carboxylate moieties from PAA/HA, whilst the bands at 1400 cm^{-1} were assigned to the O-H bending of acrylic acid), 1556 cm^{-1} for C=C stretching of the aromatic groups and 2940 cm^{-1} for the C-H stretching vibration in the polymer network. The broadening of the absorption O-H band at 3288 cm^{-1} was evident in the two-component interpenetrating PVA/PAA-HA IPN.

In Figure 4c, the widening of O-H stretching vibration in the three-component PVA/PAA-HA/P(AAm-*co*-VIm) network (between 3700 cm^{-1} and 2990 cm^{-1}) was observed in comparison to the single-component and two-component polymer networks. Moreover, the N-H stretching band of P(AAm-*co*-VIm) in the PVA/PAA-HA/P(AAm-*co*-VIm) network appeared to be superimposed by the broad O-H stretching of PVA and PAA-HA. The broadening and shift of the O-H stretching towards lower wavenumber provide us with the evidence that the PVA chains have combined with the other polymers within the network via strong hydrogen bonding. The C=O stretching of the amide groups in the three-component PVA/PAA-HA/P(AAm-*co*-VIm) network was also shifted from

1648 cm^{-1} to 1666 cm^{-1}. Comparing the FTIR spectra, the PVA/PAA-HA/P(AAm-*co*-VIm) polymer network was formed successfully. Since P(AAm-*co*-VIm) was a linear polymer chain being added to the polymer network, it was loosely bound within the IPN and most likely formed hydrogen bonding with PVA and PAA-HA via its amide and imidazole moieties.

From the FESEM micrographs, rough surfaces and porous microstructures were observed in the oven dried PVA/PAA-HA and PVA/PAA-HA/P(AAm-*co*-VIm) IPNs (Figure 5c-d), compared to the smoother surface and compact structure of the single-component PVA network (Figure 5b). Both PVA/PAA-HA and PVA/PAA-HA/P(AAm-*co*-VIm) IPNs also exhibited interconnected crosslinked three-dimensional network structures. Surface roughness indicates high surface area of the polymer adsorbents which can offer more adsorption sites for the dye molecules. These porous adsorbents tend to exhibit lower mass transfer resistance, which eventually facilitate the diffusion of dye molecules during physisorption and chemisorption [15]. Based on the photographs of the dried polymer cubes (Figure 5a), the more regular and well-shaped PVA/PAA-HA (Figure 5a-II) and PVA/PAA-HA/P (AAm-*co*-VIm) (Figure 5a-III) IPN cubes strongly suggest their enhanced bulk mechanical strength than that of the dried single-component PVA network (Figure 5a-I) with observed irregular shaped cubes.

Swelling Behaviour

Swelling behaviour is one of the major parameters in determining the removal efficiency of pollutants in water for hydrogels and polymer networks. Swelling properties of polymer networks are usually associated to the material characteristics of hydrogel networks, such as the nature of polymer, crosslinking density and chemical functionalities of the polymer hydrogels. Figure 6 illustrates the swelling behaviour of the polymer networks in two different media, which were DI water and PBS at neutral pH and under ambient conditions. The PBS was chosen as it mimics the biological electrolytes. All polymer networks showed high water absorption in DI water and PBS, thus rapid swelling rate in the first 6 h, with PVA/PAA-HA and PVA/PAA-HA/P(AAm-*co*-VIm) networks showing comparably rapid swelling rates in DI water. The swelling rate of the PVA network was the slowest among the three types of polymer networks in both media, before reaching its swelling equilibrium at 147% (PBS) and 155% (DI water) after 24 h. The three-component PVA/PAA-HA/P(AAm-*co*-VIm) IPN exhibited the highest swelling ratio at 3490% in DI water compared to the single- and two-component polymer networks (Figure 6a). In contrast, the two-component PVA/PAA-HA network exhibited the highest swelling ratio at 702% in PBS media after 24 h soaking in respective media (Figure 6b).

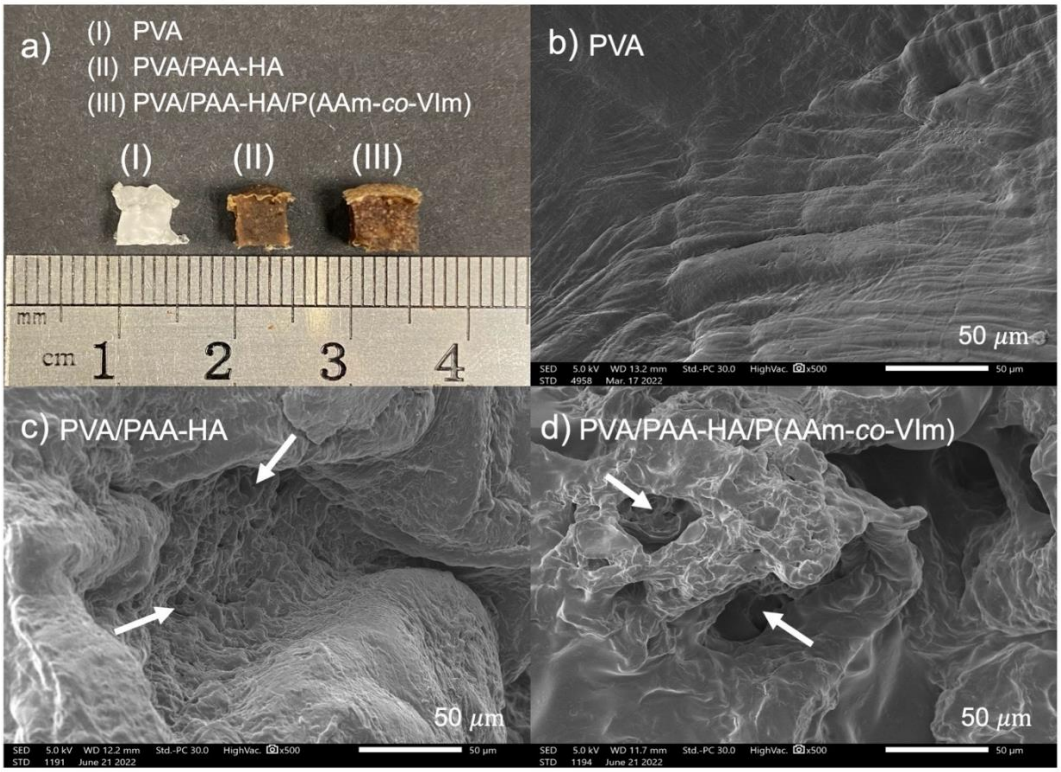

Figure 5. (a) Photographs of oven dried single-component PVA network (I), two-component PVA/PAA-HA (II) and three-component PVA/PAA-HA/P(AAm-*co*-VIm) (III) IPN. FESEM micrographs of the (b) PVA, (c) PVA/PAA-HA, and (d) PVA/PAA-HA/P(AAm-*co*-VIm) polymer networks at 500× magnification. Arrows indicate the pores in the IPNs.

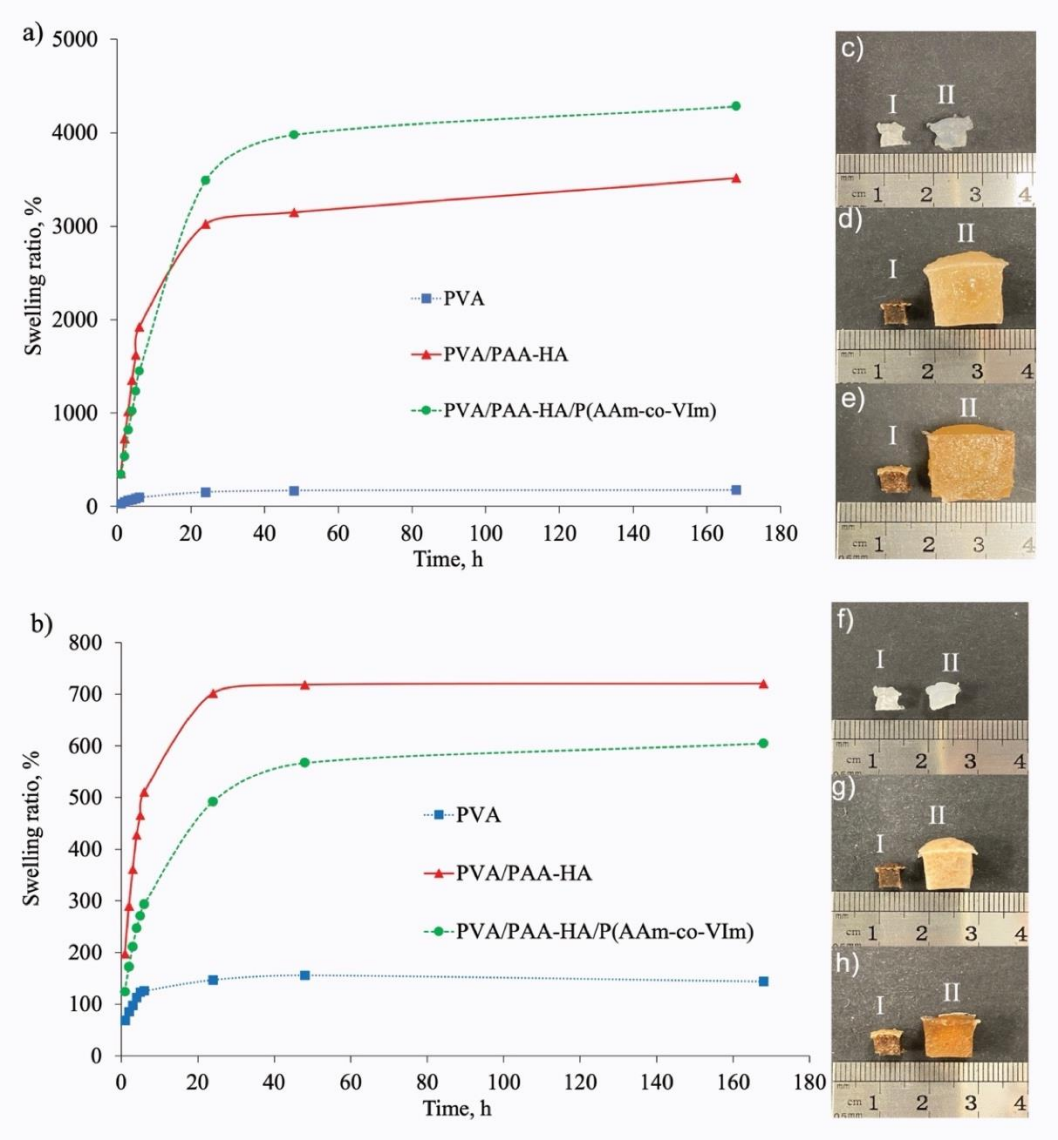

Figure 6. Swelling (%) of different polymer-based adsorbents in (a) DI water and (b) PBS at neutral pH and room temperature for 24 h. Photographs comparing the changes of polymer adsorbents before (I) and after (II) swelling in DI water for (c) the single-component PVA network; (d) two-component PVA/PAA-HA network; and (e) three-component PVA/PAA-HA/P(AAm-*co*-VIm) network. Photographs comparing the changes of polymer adsorbents before (I) and after (II) swelling in PBS for (f) the single-component PVA network; (g) two-component PVA/PAA-HA network; and (h) three-component PVA/PAA-HA/P(AAm-*co*-VIm) network.

The superabsorbent polymer systems show substantial increase in the hydrogel dimensions after swelling experiments (Figure 6c-h), especially PVA/PAA-HA and PVA/PAA-HA/P(AAm-*co*-VIm) networks, which were substantially larger than their dried states (I). The presence of abundant hydroxyl groups on the polymers attracts water molecules and make the polymer network swollen. Besides the hydroxyl groups, other hydrophilic functional groups such as acrylate, carboxylic acid, amide, imidazole and amine groups originating from the PAA-HA and P(AAm-*co*-VIm) also enhance the water absorption of the polymer networks [15]. The swelling percentages of the two-component and three-component IPNs containing PAA and PAAm were high. The PAA and PAAm are often known as superabsorbent polymers because they can absorb water many times their weights and can swell extensively due to hydrophilic moieties of the polymer chains. High swelling behaviour can favourably open up the internal pores of the polymer adsorbent, allowing better diffusion dissolved dyes to the functional sites of the polymer networks, leading to higher removal efficiency of pollutants [3].

Adsorption of Organic Dyes

The adsorbent dosage is a crucial parameter in optimizing the adsorption behaviour for various pollutants. Two adsorbent dosages, ranging between 1 g L^{-1} and 2 g L^{-1} (Table 1) were used for the adsorption of methylene blue (MB, model cationic dye) and

methyl orange (MO, anionic dye) using initial dye concentration of 250 mg L^{-1} at pH 7. The adsorption studies were carried out until adsorption equilibrium was reached under room temperature (~24 h).

Figure 7 illustrates the removal percentages for the organic dyes by using different adsorbent dosages as well as adsorption capacity (q_e) of MB using different polymer adsorbents. Our findings showed that nearly similar removal percentages for MB were achieved by using PVA/PAA-HA and PVA/PAA-HA/P(AAm-*co*-VIm) adsorbents, ranging between 91% and 94% for both adsorbent dosages. The highest MB adsorption was reported for PVA/PAA-HA (93.26%, 223.37 mg L^{-1}) and PVA/PAA-HA/P(AAm-*co*-VIm) (94.04%, 225.89 mg L^{-1}) at adsorbent dosage of 2 g L^{-1}. In contrast, only 8 – 12% MB was adsorbed by the single-component PVA adsorbents (as control) at both adsorbent dosages. Generally, organic dye adsorption increases with the amount of adsorbent used. Although slightly higher MB removal percentages were observed when a higher adsorbent dosage was used, the differences of 1 – 4% were not significant. As such, to prevent wastage of material while optimizing the removal efficiency of MB dye, 1g L^{-1} adsorbent dosage of IPN adsorbents was recommended for subsequent adsorption studies.

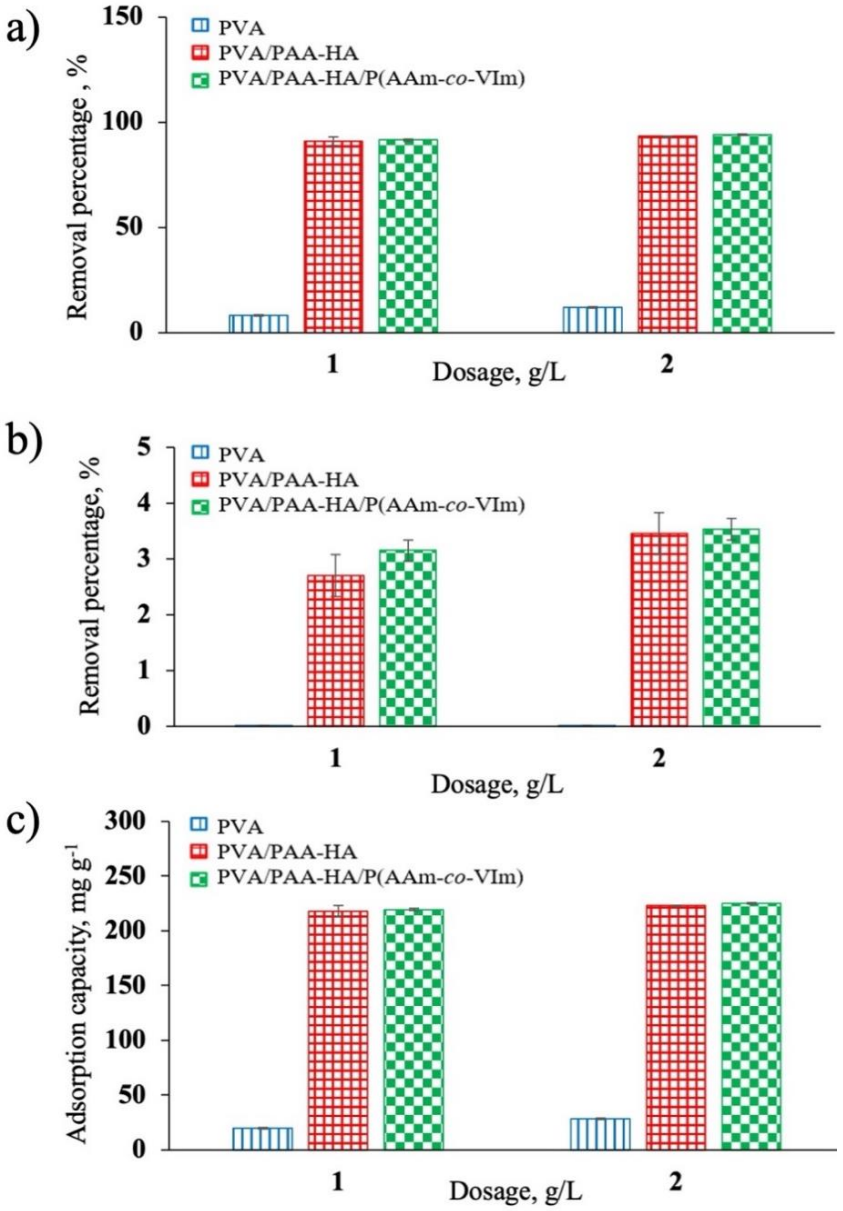

Figure 7. Effects of adsorbent dosage on the removal percentages (%) of (a) MB and (b) MO dyes at neutral pH; and (c) adsorption capacity *(q_e)* of MB by using different polymer adsorbents. The batch adsorption experiments were conducted at pH 7 using initial dye concentration of 250 mg L^{-1}. Mean values and their standard deviation values were included.

The excellent adsorption efficiency of MB dye by the two- and three-component IPN adsorbents corroborates with the substantial decrease of the blue colour intensity of the aqueous MB solutions after the dye adsorption experiments. Moreover, the dark blue-stained IPN adsorbents further confirms the MB immobilization on the surface and within the PVA/PAA-HA and PVA/PAA-HA/P(AAm-*co*-VIm) IPN adsorbents. As MB is a cationic organic dye, the MB dye could be adsorbed and trapped securely within the three-dimensional crosslinked polymer networks via strong electrostatic attractions and hydrogen bonding with the polymer adsorbents consisting of PAA-HA and P(AAm-*co*-VIm) [17-18].

The removal of negatively-charged MO dye by the PVA/PAA-HA and PVA/PAA-HA/P(AAm-*co*-VIm) IPN adsorbents were extremely low ranging between 2.50% and 3.53% (6 – 11 mg L^{-1}) for both adsorbent dosages (Figure 7b). No significant MO adsorption was observed by the PVA adsorbents. Extremely low MO adsorption was likely attributed by the electrostatic repulsion between the MO dye and the polymer adsorbents, which possess the negatively-charged PAA-HA (acrylate and humic acid groups) in neutral pH conditions. Our finding corroborates with Abidi et al. [19], who reported low removal of an anionic dye due to electrostatic repulsion between the negatively-charged adsorbent surface and the anionic molecule, especially under basic conditions (pH >10). Based on our results, the PVA/PAA-HA and PVA/PAA-HA/P(AAm-*co*-VIm) adsorbents demonstrated selective adsorption of positively-charged dye molecules. However, the adsorption of anionic dye by such negatively-charged adsorbents could be enhanced under acidic conditions (pH<4), when abundant protons from the acid could react with the negatively-charged adsorbent surface, converting the adsorbent into a neutrally- or positively-charged surface.

In this study, only the MB adsorption capacity was shown due to the extremely low MO adsorption by the IPN adsorbents used. In Figure 7a, only a small increase in the MB removal (< 2%) was observed with increasing adsorbent dosage. At higher adsorbent dosage and a fixed initial MB concentration, the MB adsorption might have reached equilibrium faster compared to the MB adsorption at a lower adsorbent dosage due to the existence osmotic pressure despite having more active adsorptive sites. Furthermore, accumulation of the cationic dye molecule within the adsorbents with time prevents more MB molecules from binding effectively to the available sites due to electronic repulsions among adjacent MB molecules, resulting in nearly similar removal percentages and adsorption capacities for 1 and 2 g L^{-1} adsorbent dosages of the PVA/PAA-HA and PVA/PAA-HA/P(AAm-*co*-VIm) adsorbents. This finding reiterates that an incompatible ratio of adsorbent dosage (active binding sites) to adsorbate could lead to an unfavourably low adsorption capacity (q_e, mg g^{-1}) of an adsorbent. Therefore, the adsorbent dosage is an important parameter to optimize the dye adsorption behaviour of the adsorbents [3].

Adsorption Kinetics for MB Dye

Kinetic studies are key in understanding time-dependent adsorption and the adsorption rate of dyes in solution by a specific adsorbent. Figures 8a and 8d show the time-dependent adsorption of MB dye by the PVA/PAA-HA and PVA/PAA-HA/P(AAm-*co*-VIm) IPN adsorbents up to 1440 min (at 298 K), respectively. The MB removal increased with increasing contact time as expected for each adsorbent and their adsorption equilibria (q_e) were reached after 18 - 24 h. Hence, subsequent adsorption experiments were carried out for 24 h to ensure equilibrium was reached.

Surprisingly, the adsorption kinetics of the PVA/PAA-HA and PVA/PAA-HA/P(AAm-*co*-VIm) were different, most likely attributed to the presence of P(AAm-*co*-VIm) copolymer in the three-component network. A rapid MB adsorption was observed for the PVA/PAA-HA adsorbent in the first 180 min, which gradually slowed down, plateauing at 18 h (Figure 8a). In comparison, much slower adsorption rate was observed in PVA/PAA-HA/P(AAm-*co*-VIm) up to 500 min, and the adsorption increased rapidly between 500 – 1200 min, before reaching its near equilibrium at 1440 min (Figure 8d). These time-dependent adsorption patterns coincide with the swelling properties of these adsorbents (Figure 6a): the PVA/PAA-HA exhibited higher swelling rate in DI water than that of PVA/PAA-HA/P(AAm-*co*-VIm) in the first 10 h, thus allowing enhanced diffusion of dye-containing solution into the PVA/PAA-HA hydrogel, trapping more dye ions to its binding sites. It was also observed that the MB adsorption onto the PVA/PAA-HA and PVA/PAA-HA/P(AAm-*co*-VIm) hydrogels occurred in three different stages at different rates (Figures 8a and 8d). An initial rapid adsorption occurred on the external surface of the adsorbents, followed by gradual dye adsorption which was possibly controlled by intra-particle diffusion and a final equilibrium stage where the intra-particle diffusion slowed down owing to the low concentration of MB dye in the solution and decreased availability of adsorption sites [20].

In this study, two classical pseudo-first order and pseudo-second order models were applied to model our kinetics datasets [21-23]. Linear regression method is widely applied in the calculations of the model parameters, owing to its simplicity [22].

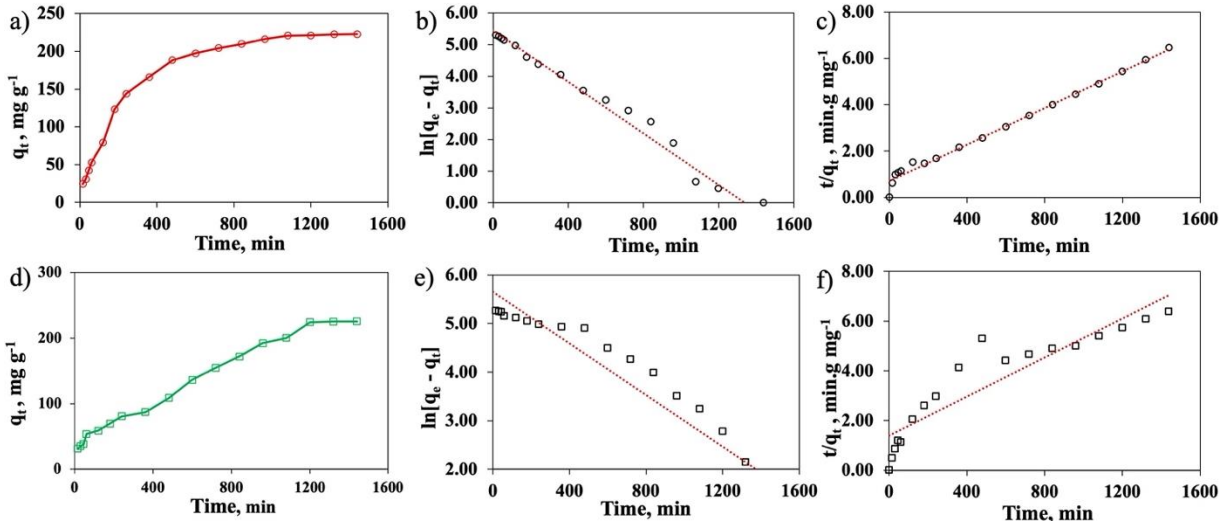

Figure 8. (a) The time-dependent adsorption of MB for PVA/PAA-HA adsorbents and its (b) the pseudo-first and (c) pseudo-second kinetic rates analysis. (d) The time dependent adsorption of MB for the PVA/PAA-HA/P(AAm-*co*-VIm) adsorbents and its (e) the pseudo-first and (f) pseudo-second kinetic rates analysis.

The linearized equations for these pseudo-first order (Equation 4) and pseudo-second order (Equation 5) models are expressed below:

$$\ln(q_e - q_t) = \ln q_e - k_1 t \qquad \text{Equation 4}$$

$$\frac{t}{q_t} = \frac{1}{k_2 q_{e2}} + \frac{1}{q_e} t \qquad \text{Equation 5}$$

where, q_t is the amount of adsorbate adsorbed (mg g^{-1}) at time t (min) and q_e is the maximum adsorption capacity (mg g^{-1}). k_1 (mg g^{-1}min^{-1}) is the pseudo-first order rate constant and k_2 (g mg^{-1}min^{-1}) is the pseudo-second order rate constant.

Kinetic linear plots and model parameters for MB adsorption by using two types of IPN adsorbents were determined and compared (Table 2). The pseudo-second order kinetic equation was more suitable for calculating the maximum adsorption capacity, $q_{e,cal}$ (mg g^{-1}) for MB at different initial concentrations because the calculated values were more consistent and closer to the experimental values ($q_{e,exp}$). Furthermore, the correlation coefficients (R^2) of the pseudo-second order model using the PVA/ PAA-HA and PVA/PAA-HA/P(AAm-*co*-VIm) adsorbents were 0.9887 and 0.8444, respectively, which were higher than R^2 values of their pseudo- first order model parameters. Therefore, the kinetics of MB adsorption by the IPN adsorbents correspond with the pseudo-second order rate and the fitting effects of the two adsorbents follow this trend: PVA/PAA-HA > PVA/PAA-HA/P(AAm-*co*-VIm). These results indicate that the MB adsorption onto the IPN adsorbents are based on chemisorption, which is mainly

Table 2. Kinetic model parameters for MB adsorption onto the PVA/PAA-HA and PVA/PAA-HA/P(AAm-*co*-VIm) IPN adsorbents at 298 K for 24 h.

	Type of adsorbents	
	PVA/PAA-HA	PVA/PAA-HA/P(AAm-*co*-VIm)
Experimental adsorption capacity, $q_{e,exp}$ (mg g^{-1})	221.91	225.65
Pseudo first-order		
Linear regression	$y = -0.0041x + 5.4561$	$y = -0.0027x + 5.6489$
$q_{e,cal}$ (mg g^{-1})	234.18	283.98
k_3 (mg g^{-1}min^{-1})	0.0041	0.0027
R^2	0.9733	0.8346
Pseudo second-order		
Linear regression	$y = 0.004x + 0.6976$	$y = 0.0039x + 1.4017$
$q_{e,cal}$ (mg g^{-1})	250.00	256.41
k_4 (g mg^{-1}min^{-1})	2.2936×10^{-5}	1.0851×10^{-5}
R^2	0.9887	0.8444

driven by electrostatic interactions between the negatively-charged IPN adsorbents and cationic MB molecule as well as electron exchange/sharing between the adsorbent and adsorbate [20, 24, 25].

Adsorption Isotherms for MB Dye

The MB dye adsorption equilibrium processes by two- and three-component IPN adsorbents were probed by using the frequently used Langmuir and Freundlich isotherm models to understand the relationship between the adsorbents and adsorbates at a specified temperature [25]. The Langmuir model assumes a monolayer sorption and energetically homogeneous binding sites. The linearised Langmuir isotherm is expressed as Equation 6:

$$\frac{C_e}{q_e} = \frac{C_e}{q_{max}} + \frac{1}{q_{max}K_L} \qquad \text{Equation 6}$$

where, C_e is the equilibrium concentration of MB (mg L^{-1}), q_e is the equilibrium adsorption capacity (mg g^{-1}), q_{max} is the maximum adsorption capacity at monolayer (mg g^{-1}) and K_L (L mg^{-1}) is the Langmuir adsorption equilibrium constant related to affinity of binding sites.

The linearised Freundlich model, which assumes that the adsorption process occurs on multilayers and heterogenous binding sites, is given in Equation 7:

$$\log q_e = \frac{1}{n}\log C_e + \log K_f \qquad \text{Equation 7}$$

where, K_f ($mg^{(1-\frac{1}{n})} \cdot L^{\frac{1}{n}} g^{-1}$) is the adsorption capacity, q_e is the adsorption capacity at equilibrium and n (L mg^{-1}) is the Freundlich constant related to the intensity of adsorption. When $\frac{1}{n} < 1$, chemisorption occurs; however, when $1 < n < 10$ is observed, physisorption is favoured.

The Langmuir and Freundlich isotherm model plots and parameters for MB adsorption onto the PVA/PAA-HA and PVA/PAA-HA/P(AAm-*co*-VIm) IPN adsorbents at 298K and neutral pH are shown in Figure 9 and Table 3. The experimental data of linearised Langmuir adsorption parameters showed negative intercepts and slopes for the PVA/PAA-HA adsorbent, suggesting that the adsorption behaviour of the tested system did not obey the Langmuir assumptions. Moreover, the R^2 value was also extremely unfavourable (0.1700). The fitting of the PVA/PAA-HA data using the Freundlich isotherm equation yielded an R^2 value of 0.9294, hence, the Freundlich isotherm model was found to be a better fit than the Langmuir model based on the regression coefficient values. With the heterogeneity factor (n) less than 1 (Table 3), the MB adsorption process occurred on the PVA/PAA-HA hydrogel was reasonably heterogenous in nature [26].

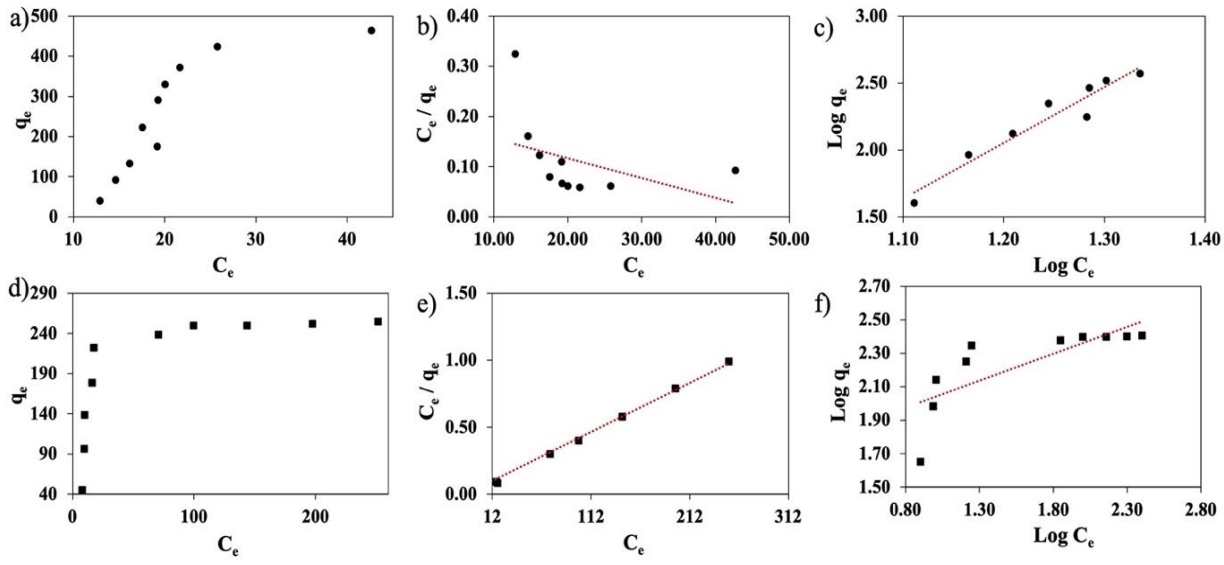

Figure 9. (a) The MB adsorption at different MB initial concentrations using the PVA/PAA-HA IPN adsorbents; and (b) the Langmuir and (c) the Freundlich isotherm models for the PVA/PAA-HA IPN adsorbents. (d) The MB adsorption at different MB initial concentrations using the PVA/PAA-HA/P(AAm-*co*-VIm) IPN adsorbents; and (e) the Langmuir and (f) the Freundlich isotherm models for the PVA/PAA-HA/P(AAm-*co*-VIm) IPN adsorbents.

Table 3. The linearised Langmuir and Freundlich adsorption isotherm parameters for MB onto the PVA/PAA-HA and PVA/PAA-HA/P(AAm-*co*-VIm) IPN adsorbents at 298 K.

Adsorbent	Langmuir I			Freundlich		
	q_{max} (mg g^{-1})	K_L (L mg^{-1})	R^2	K_f (mg$^{(1-\frac{1}{n})}$ · L$^{\frac{1}{n}}$ g^{-1})	n (L mg^{-1})	R^2
PVA/PAA-HA	-250.00	-0.0204	0.1700	0.0011	0.2401	0.9294
PVA/PAA-HA/P(AAm-*co*-VIm)	270.27	0.0680	0.9872	52.3359	3.1075	0.5893

Interestingly, the MB adsorption onto the PVA/PAA-HA/P(AAm-*co*-VIm) adsorbent obeyed the Langmuir isotherm model, with high R^2 value of 0.9872 compared to that of the Freundlich isotherm fitting (R^2 = 0.5893). The calculated K_L value was less than 1, which indicated that the interactions between MB and the PVA/PAA-HA/P(AAm-*co*-VIm) adsorbent was most possibly involving monolayer and localized adsorption [24]. To further investigate the characteristics of the Langmuir adsorption model, a dimensionless constant, R_L, was calculated based on Equation 8 [20, 25]:

$$R_L = \frac{1}{(1+K_L C_o)} \quad \text{Equation 8}$$

where, C_o is the initial MB concentration (mg L^{-1}) and K_L (L mg^{-1}) is the Langmuir adsorption equilibrium constant. The R_L indicates that the adsorption process tends to be unfavourable ($R_L > 1$), linear ($R_L = 1$), favourable ($0 < R_L < 1$), or irreversible ($R_L = 0$). Smaller R_L values suggest high affinity between the adsorbent and the adsorbate. Since our calculated R_L values for MB were less than 1 for the initial MB concentrations ranging between 50 - 500 mg L^{-1}, a highly favourable adsorption process for MB onto the PVA/PAA-HA/P(AAm-*co*-VIm) adsorbent was anticipated.

CONCLUSION

In conclusion, sodium humate-grafted poly(acrylic acid) (PAA-HA) and poly(acrylamide-*co*-1-vinyl imidazole) (P(AAm-*co*-VIm)) were successfully synthesized via free-radical polymerization with high yields. Two superabsorbent IPNs consisting of PAA-HA, P(AAm-*co*-VIm) and poly(vinyl alcohol) (PVA) were facilely assembled at predetermined weight ratios in aqueous solutions and cyclic freeze-thawed, yielding strong and stable hydrogels. It is worth noting that the IPN adsorbents exhibited porous microstructures and excellent swellability in aqueous media (>3000% in DI water) at neutral pH, contributing to their high MB dye removal percentages (91 – 94%) and rapid adsorption rates and reached adsorption equilibria at 24 h under similar experimental conditions. Maximum MB adsorption capacities at pH 7 for both PVA/PAA-HA and PVA/PAA-HA/P(AAm-*co*-VIm) ranged between 220 mg g^{-1} and 225 mg g^{-1} for the two adsorbent dosages used (1 g L^{-1} and 2 g L^{-1}). Based on the extremely low removal percentages of MO dye, which is an anionic dye, it is concluded that the IPN adsorbents demonstrated selective adsorption toward positively-charged species, such as MB dye, owing to highly negatively-charged surfaces containing PAA-HA.

The MB adsorption of the IPN hydrogels followed pseudo-second order kinetic model, suggesting that the key adsorption mechanism was chemisorption based on electrostatic interactions and electron exchange/sharing. It is fascinating to observe that the IPN adsorbents exhibited different adsorption isotherms on account of P(AAm-*co*-VIm) incorporation in the three-component system: the MB adsorption process of PVA/PAA-HA corresponded to the Freundlich model indicating a more heterogenous process; whereas the Langmuir model parameters were more suitable to describe the monolayer adsorption process involving PVA/PAA-HA/P(AAm-*co*-VIm).

ACKNOWLEDGEMENTS

This study was funded by the Sustainable Development Goals Borneo (SDG Borneo) Research Grant (600-RMC/SDG-Borneo 5/3 (012/2020). The authors would like to thank Chin Ann Yap of Malaysian Pepper Board for his technical assistance in the sample lyophilization.

REFERENCES

1. Lim, J. Y., Goh, S. S., Liow, S. S., Xue, K. & Loh, X. J. (2019) Molecular gel sorbent materials for environmental remediation and wastewater treatment. *Journal of Materials Chemistry A*, **7(32)**, 18759–18791.

2. Yao, G., Bi, W. & Liu, H. (2020) pH-responsive magnetic graphene oxide/poly (NVI-co-AA) hydrogel as an easily recyclable adsorbent for cationic and anionic dyes. *Colloids and Surfaces A: Physicochemical and Engineering Aspects*, **588**, 124393.

3. Hu, X. S., Liang, R. & Sun, G. (2018) Super-adsorbent hydrogel for removal of methylene

blue dye from aqueous solution. *Journal of Materials Chemistry A*, **6(36)**, 17612–17624.

4. Karim, S., Ahmad, N., Hussain, D., Mok, Y. S. & Siddiqui, G. U. (2022) Active removal of anionic azo dyes (MO, CR, EBT) from aqueous solution by potential adsorptive capacity of zinc oxide quantum dots. *Journal of Chemical Technology & Biotechnology*, **97(8)**, 2087-2097.

5. Dutta, S., Gupta, B., Srivastava, S. K. & Gupta, A. K. (2021) Recent advances on the removal of dyes from wastewater using various adsorbents: A critical review. *Materials Advances*, **2**, 4497–4531.

6. Ali, I. (2012) New generation adsorbents for water treatment. *Chemical Reviews*, **112(10)**, 5073–5091.

7. Sabzehmeidani, M. M., Mahnaee, S., Ghaedi, M., Heidari, H. & Roy, V. A. (2021) Carbon based materials: A review of adsorbents for inorganic and organic compounds. *Materials Advances*, **2(2)**, 598–627.

8. Nazarzadeh Zare, E., Mudhoo, A., Ali Khan, M., Otero, M., Bundhoo, Z. M. A., Patel, M., Srivastava, A., Navarathna, C., Mlsna, T., Mohan, D. and Pittman Jr, C. U., Makvandi & P., Sillanpää, M. (2021) Smart adsorbents for aquatic environmental remediation. *Small*, **17(34)**, 2007840.

9. Alipoori, S., Rouhi, H., Linn, E., Stumpfl, H., Mokarizadeh, H., Esfahani, M. R. & Wujcik, E. K. (2021) Polymer-based devices and remediation strategies for emerging contaminants in water. *ACS Applied Polymer Materials*, **3(2)**, 549–577.

10. Godiya, C. B., Ruotolo, L. A. M. & Cai, W. (2020) Functional biobased hydrogels for the removal of aqueous hazardous pollutants: current status, challenges, and future perspectives. *Journal of Materials Chemistry A*, **8(41)**, 21585–21612.

11. Dragan, E. S. (2014) Design and applications of interpenetrating polymer network hydrogels. A review. *Chemical Engineering Journal*, **243**, 572–590.

12. Hu, N., Chen, C., Tan, J., Wang, W., Wang, C., Fan, H., Wang, J., Müller-Buschbaum, P. & Zhong, Q. (2020) Enhanced adsorption of methylene blue triggered by the phase transition of thermos-responsive polymers in hybrid interpenetrating polymer network hydrogels. *ACS Applied Polymer Materials*,**2(8)**, 3674–3684.

13. Sarmah, D. & Karak, N. (2020) Double network hydrophobic starch based amphoteric hydrogel as an effective adsorbent for both cationic and anionic dyes. *Carbohydrate Polymers*, **242**, 116320.

14. He, Y., Bao, W., Hua, Y., Guo, Z., Fu, X., Na, B., Yuan, D., Peng, C. & Liu, H. (2022) Efficient adsorption of methyl orange and methyl blue dyes by a novel triptycene-based hyper-crosslinked porous polymer. *RSC Advances*, **12(9)**, 5587–5594.

15. Pour, Z. S. & Ghaemy, M. (2015) Removal of dyes and heavy metal ions from water by magnetic hydrogel beads based on poly (vinyl alcohol)/carboxymethyl starch-g-poly (vinyl imidazole). *RSC Advances*, **5(79)**, 64106–64118.

16. Das, D., Ghosh, P., Dhara, S., Panda, A. B. & Pal, S. (2015) Dextrin and poly (acrylic acid)-based bio- degradable, non-cytotoxic, chemically cross-linked hydrogel for sustained release of ornidazole and ciprofloxacin. *ACS Applied Materials & Interfaces*, **7(8)**, 4791–4803.

17. Lv, Q., Shen, Y., Qiu, Y., Wu, M. & Wang, L. (2020) Poly (acrylic acid)/poly (acrylamide) hydrogel adsorbent for removing methylene blue. *Journal of Applied Polymer Science*, **137(43)**, 49322.

18. Yi, J. Z. & Zhang, L. M. (2008) Removal of methylene blue dye from aqueous solution by adsorption onto sodium humate/polyacrylamide/ clay hybrid hydrogels. *Bioresource Technology*, **99(7)**, 2182–2186.

19. Abidi, N., Duplay, J., Jada, A., Errais, E., Ghazi, M., Semhi, K. and Trabelsi-Ayadi, M. (2019) Removal of anionic dye from textile industries' effluents by using Tunisian clays as adsorbents. Zeta potential and streaming-induced potential measurements. *Comptes Rendus Chimie*, **22(2-3)**, 113–125.

20. Niu, Y., Han, X., Huang, L. & Song, J. (2020) Methylene blue and lead (II) removal via degradable interpenetrating network hydrogels. *Journal of Chemical & Engineering Data*, **65(4)**, 1954–1967.

21. Ho, Y. S. & McKay, G. (1999) Pseudo-second order model for sorption processes. *Process Biochemistry*, **34(5)**, 451–465.

22. Wang, J. & Guo, X. (2020) Adsorption kinetic models: Physical meanings, applications, and solving methods. *Journal of Hazardous Materials*, **390**, 122156.

23. Revellame, E. D., Fortela, D. L., Sharp, W., Hernandez, R. & Zappi, M. E. (2020) Adsorption

kinetic modeling using pseudo-first order and pseudo-second order rate laws: A review. *Cleaner Engineering and Technology*, **1**, 100032.

24. Chen, L., Li, Z., Li, W., Chen, Z., Chen, G., Yang, W., Zhang, X. & Liu, X. (2021) Investigation of adsorption kinetics and the isotherm mechanism of manganese by modified Diatomite. *ACS Omega*, **6(25)**, 16402–16409.

25. Jiang, L., Wen, Y., Zhu, Z., Liu, X. & Shao, W. (2021) A Double cross-linked strategy to construct graphene aerogels with highly efficient methylene blue adsorption performance. *Chemosphere*, **265**, 129169.

26. Zaidi, R., Khan, S. U., Farooqi, I. H. & Azam, A. (2021) Investigation of kinetics and adsorption isotherm for fluoride removal from aqueous solutions using mesoporous cerium–aluminum binary oxide nanomaterials. *RSC Advances*, **11(46)**, 28744–28760.